Proceedings of the 27th International Symposium on Power Semiconductor Devices & IC's
May 10-14, 2015, Kowloon Shangri-La, Hong Kong

Design and optimization of GaN Lateral Polarization-doped Super-Junction (LPSJ): an analytical study

Bo Song[1,2*], Mingda Zhu[2], Zongyang Hu[2], Kazuki Nomoto[2], Debdeep Jena[1,2,3] and Huili (Grace) Xing[1,2,3*]
[1]School of Electrical and Computer Engineering, Cornell University, Ithaca, NY 14853, USA
[2]Department of Electrical Engineering, University of Notre Dame, Notre Dame, IN 46556, USA
[3]Department of Materials Science and Engineering, Cornell University, Ithaca, NY 14853, USA
Email: bs728@cornell.edu and hgx2@cornell.edu

***Abstract*— A 2D analytical model for breakdown voltage (BV) and specific on-resistance ($R_{on,sp}$) of GaN lateral polarization-doped super-junction (LPSJ) devices has been developed. The electric field along the critical path has been modeled and compared with 2D simulation results, followed by breakdown voltage calculation using impact ionization integral. Design space and optimization of LPSJ has been disused in terms of n/p pillar doping, thickness and aluminum composition x_{Al} in grading AlGaN. The 2D analytical model represents a more realistic performance limit than the 1D model and the $R_{on,sp}$ of LPSJ with x_{Al} = 0.3 shows > 10x reduction over conventional GaN junctions for BV>2 kV. It can provide useful guidelines for the development of LPSJ and the design criteria to achieve minimum $R_{on,sp}$.**

Keywords—Super-junctoin; Polarization; GaN; Breakdown voltage; Specfic On resistance; Analytical

I. INTRODUCTION

GaN based power devices has attracted great attentions due to its high breakdown field and high electron mobility. Remarkable progresses on GaN based power devices have been achieved recently by several groups on GaN-on-Si or GaN-on-GaN platform [1-4], on the way to approach the unipolar limit of breakdown voltage and on resistance of GaN material. Super-junction concept, which based on charge compensation in the drift region by fully balanced n and p pillar region, has been widely adopted in Si power device to break such tradeoff of breakdown voltage and on resistance [5-7]. Thus the combination of advantage of GaN material and super-junction concept would further improve GaN based device performance. GaN super junction devices using impurity doping [8] or natural super junction [9] based on the polarization sheet charge have been studied to beat the aforementioned limit. However, impurity doping to form p type pillar in GaN still remains a great challenge due to the high activation of Mg in GaN (~200 meV); furthermore, practical solutions for device fabrication has also not been proposed yet. The natural super junction has a high electric field crowding problem due to the high sheet charge of the 2 dimension electron gas (2DEG) and 2 dimension hole gas (2DHG), thus only device performance far less than expected has been reported to date. Recently, we proposed lateral polarization-doped super junction (LPSJ) as shown in Fig.1 (a): the n/p pillar regions are realized by compositionally grading AlGaN [10], where the electron and hole concentrations are uniform and balanced in the n/p pillar regions.

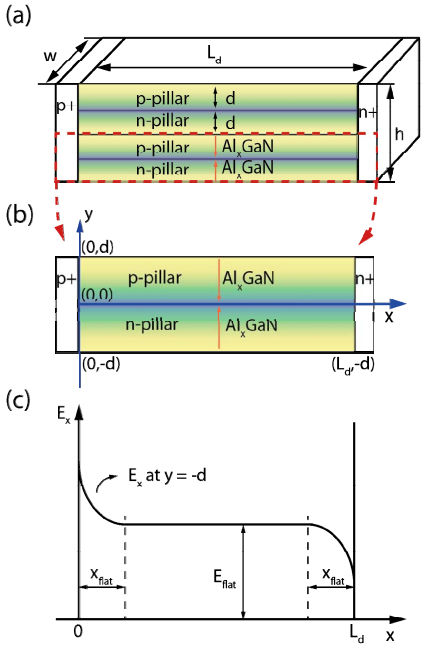

Fig. 1: (a) Schematic view of the LPSJ structure, (b) the unit cell of LPSJ, (c) the electric field distribution along the x direction at $y = -d$ in a LPSJ showing the peak field E_{max} occurs at $x=0$.

In this paper, a 2D analytical modeling of the electric field and breakdown voltage of GaN LPSJs is presented. Design optimization in terms of the n/p pillar doping, thickness and x_{Al} composition are discussed.

II. LATERAL POLARIZATION-DOPED SUPER-JUNCTION

The LPSJ features uniformly doped n/p pillar regions by lineally grading the Al composition x_{Al} up and down in the Al_xGaN layers alternatively [11], [12], and the n+ and p+ cathode/anode regions are formed by regrowth to connect with the n and p pillars, respectively[13], [14]. The unit cell of the LPSJ is shown in Fig.1 (b), where both n and p pillars have a thickness of d, the length of the drift region is L_d , the doping concentrations can be expressed as

$$n=p=N_a=N_d=\sigma_\pi/d \quad (1)$$

where σ_π is the net polarization charge in Al_xGaN (cm^{-2}). So the unit cell, consisting of a pair of n/p pillars with balanced charges shown in Fig.1 (b), can be treated in the same fashion as traditional p-n super-junction in terms of electric field profile modeling. When the LPSJ is under reverse bias, there is depletion in the n/p pillars in both lateral and vertical directions, eventually leading to a full depletion in the drift region. Due to the symmetry of LPSJ, the electric field profile is symmetric along the center line of the structure. Strollo et al. established an exact analytical solution for the electric field along $y=-d$ when n/p pillars are fully depleted[15],

$$E(x)|_{y=-d}=-2\frac{V^* x}{L_d^{\,2}}+\frac{V_r+V^*}{L_d}+\sum_{n=1}^{\infty}\frac{K_n\gamma_n}{2}\frac{\cos(K_n x)}{\cosh(K_n(-d))} \quad (2)$$

where $V^*=(qN/2\varepsilon_s)L_d^{\,2}$ $K_n=n\pi/L_d$, $\gamma_n=8V^*/(n\pi)^3\left[(-1)^n-1\right]$ $\gamma_n=8V^*/(n\pi)^3\left[(-1)^n-1\right]$ and V_r is the applied revered voltage. The schematic electric field profile along the x direction at $y = -d$ is also showing in Fig.1(c), where the peak maximum electric field E_{max} occurs at $x = 0$ and $y = -d$. When $0< d/L_d <1$, which will be the case in our discussion where the thin n and p pillar can be easily controlled by the MBE/MOCVD epitaxy growth, the maximum electric field at $x = 0$ can be approximated to be[16]

$$E_{\max}=E_{flat}+\frac{qN}{2\varepsilon_s}\times 1.66d \ , \quad (3)$$

where $E_{flat}=\frac{V_r}{L_d}$, which is from the flat electric filed distribution when n/p are fully depleted (Fig. 1c), thus it can treated as the electric filed in the i-region of a PIN diode.

In order to calculate the breakdown voltage, we need to use the ionization integral along the critical electric field path (i.e. the peak electric field path), where using Eq.2 can be challenging. On the other hand, this electric field profile can be also modeled using a polynomial approximation [17]

$$E=\begin{cases} E_{flat}+\dfrac{qN}{\varepsilon_s}\cdot\dfrac{(x-x_{flat})^m}{m x_{flat}^{\,m-1}}, x\in[0,x_{flat}] \\ E_{flat}, x\in[x_{flat},L_d-x_{flat}] \\ E_{flat}-\dfrac{qN}{\varepsilon_s}\cdot\dfrac{(x-x_{flat})^m}{m x_{flat}^{\,m-1}}, x\in[L_d-x_{flat},L_d] \end{cases} \quad (4)$$

The maximum electric field along $y = -d$ is at $x = 0$

$$E_{\max}=E_{flat}+\frac{qN}{\varepsilon_s}\times\frac{x_{flat}}{m} \quad (5)$$

Comparing the E_{max} expressions in Eq.2 and Eq.5, we can get

$$x_{flat}=0.83md \quad (6)$$

The only fitting parameter m can be obtained by fitting the electric field profile simulated by Sentaurus. For a range of feasible N_d and d values, m = 3 resulted in the best fitting (Fig.2). Thus, we can find the electric field along $y = -d$

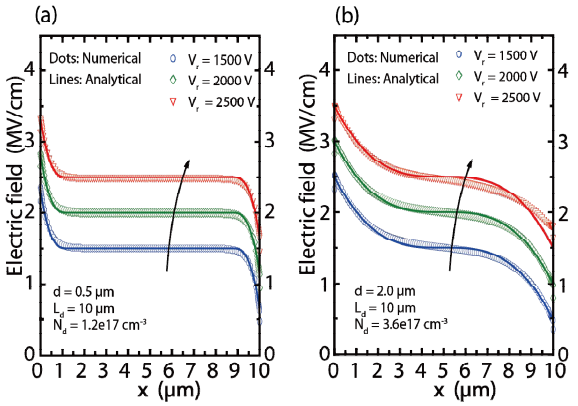

Fig.2: Electric filed distribution comparison between modeled and numerical simulation along $y=-d$ under different d, N_d values where L_d =10 μm: (a) d = 0.5 μm, N_d= 1.2x10^{17} cm^{-3} and (b) d = 2 μm, N_d= 3.6x10^{16} cm^{-3}

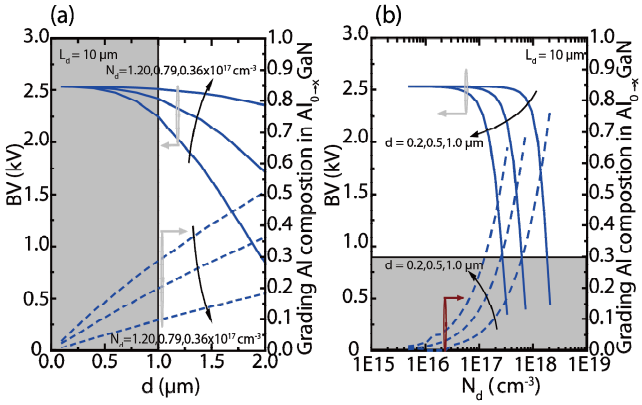

Fig.3: Breakdown voltage dependence on (a) pillar width d and (b) doping concentration N_d and its associated x_{Al} at L_d =10 μm. Breakdown voltage reduces with higher doping and larger pillar width. The shaded region ($d \le 1$ μm, $x_{Al} \le 0.3$) denotes our feasible growth region at present.

$$E=\begin{cases} E_{flat}+\dfrac{qN}{\varepsilon_s}\cdot\dfrac{(x-x_{flat})^3}{3x_{flat}^{\,2}}, x\in[0,x_{flat}] \\ E_{flat}, x\in[x_{flat},L_d-x_{flat}] \\ E_{flat}-\dfrac{qN}{\varepsilon_s}\cdot\dfrac{(x-x_{flat})^3}{3x_{flat}^{\,2}}, x\in[L_d-x_{flat},L_d] \end{cases} \quad (7)$$

The breakdown voltage (BV) can then be found by solving the impact ionization integral

$$\int_0^{L_d}\alpha dx=1 \quad (8)$$

where impact ionization rate $a=1.5\times10^{-42}E^7$ is used [18].

The $R_{on,sp}$ of the LPSJ considering only unipolar current conducting in the undepleted n pillar region can be expressed as

$$R_{on,sp}=\frac{L_d^{\,2}}{q\mu N_d}\frac{2d}{h(d-d_{dep})} \quad (9)$$

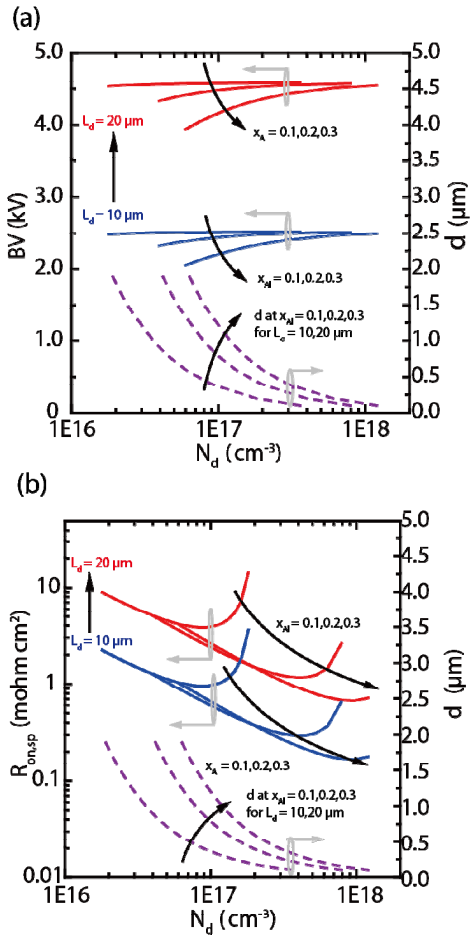

Fig.4: (a) Breakdown voltage BV and (b) $R_{on,sp}$ dependence on N_d for various Al_xGaN (x_{Al} = 0.1, 0.2, 0.3) and L_d (10, 20 μm) with the total pillar height h = 4 μm. The dashed lines depict the associated pillar thickness d. BV slightly increases with smaller d and higher N_d. $R_{on,sp}$ reduces with increasing x_{Al}. A minimum $R_{on,sp}$ is observed with respect to doping, mobility, and effective conducting area for a given x_{Al}.

where $\bar{\mu}$ is the average mobility in the graded AlGaN layer, h is the total height of the LPSJ pillar stacks and d_{dep} is the depletion region in the n pillar region

$$d_{dep} = \sqrt{\frac{2\varepsilon_s V_{bi}}{q}\left(\frac{1}{N_a}+\frac{1}{N_d}\right)} \tag{10}$$

where V_{bi} is the built in potential

$$V_{bi} = \frac{K_B T}{q} In\left(\frac{N_a N_d}{n_i^2}\right) \tag{11}$$

III. Resutls and Discussion

The BV dependence on the pillar width d, doping concentration N_d and the associated x_{Al} is shown in Fig 3 for a fixed drift region length L_d=10 μm. BV is lower for both larger d and higher N_d, which is expected because the n/p pillars are hard to be fully depleted, thus the super-junction will act more like a traditional abrupt pn junction with field crowding at the

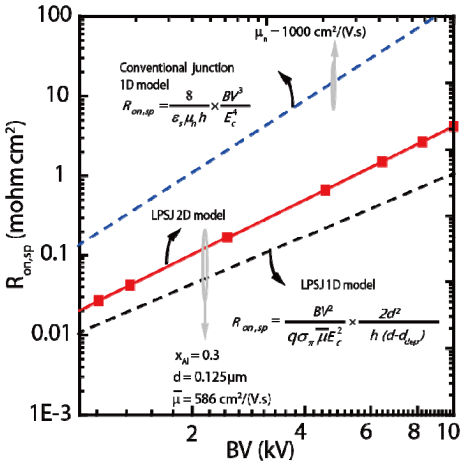

Fig.5: Comparison of R_{onsp}-BV between GaN conventional junction with 1D model and LPSJ with 1D and 2D model. LPSJ 2D model shows >10x reduction in $R_{on,sp}$ over conventional junction for BV > 2 kV, and a more accurate performance limit over LPSJ 1D model.

P+/N and N+/P junctions, thus leading to lower BV. Since the doping of the n/p pillar region is controlled by the Al composition in the Al_xGaN, with a higher doping and larger pillar width, a high x_{Al} is needed to get the associated charge. The x_{Al} value at the corresponding doping and pillar width is also shown in Fig.3. For example, with a doping of 1.2×10^{17}cm^{-3} and a pillar width of 2 μm, we need to grade from GaN to $Al_{0.5}GaN$ over 2 μm. While based on our ongoing experimental development, grading a high Al composition over a thick layer is challenging. The shaded region with $d \le 1$ μm and $x_{Al} \le 0.3$ in Fig.3 denotes the practical design space based on the known device epitaxial growth conditions today.

Besides dialing the traditional knobs such as the doping and pillar thickness, the Al composition x_{Al} of the Al_xGaN is other unique parameter we can adjust. Figure 4 (a) shows the calculated BV for 3 different x_{Al} values 0.1 to 0.3 while varying d to change N_d. BV is slightly higher with a smaller d and a higher N_d for a lower x_{Al} where the total charge is low and the fully depletion can be easy to meet. While for a higher x_{Al}, the total charge in the n/p pillar is higher, and along with a larger pillar width, full depletion is difficult to reach before the device breaks down. As a result, we see a large change in BV when the pillar width increases from 0.1 to 2 μm. For example, BV is found to be ~2050 V for $N_d = 6\text{x}10^{16}$ cm^{-3}, d =2 μm and increases to ~2500 V for $N_d = 1.2\times10^{18}$ cm^{-3}, d = 0.1 μm, while x_{Al} is 0.3 and L_d =10 μm. Since the effective electron mobility in the graded layer depends on the Al composition and the resultant doping concentration, an average mobility considering the alloy scattering and optical phonon scattering is used to model $R_{on,sp}$ as shows in Fig.4(b). The overall trend is that with a higher x_{Al} composition, a lower $R_{on,sp}$ can be obtained since it results in a higher carrier concentration in the conducting pillars though the electron mobility is lower due to the enhanced alloy scattering. Besides, $R_{on,sp}$ shows a minimum for a given x_{Al} due to the tradeoff among doping concentration, carrier mobility and effective conducting area.

The tradeoff relationship between BV and $R_{on,sp}$ for conventional GaN impurity-doped junctions and LPSJ with the 1D (simplified [10]) and 2D (improved, this work) analytical model is compared in Fig.5. For instance, the $R_{on,sp}$ of LPSJ with x_{Al} = 0.3 shows > 10x reduction over conventional junctions for BV > 2 kV. Since the 2D analytical model represents a more realistic performance limit than the simplified 1D model, which is attributed to a more accurate modeling of the electric field and calculating BV by impact ionization integral, it provides useful guidelines for the development of LPSJ and the design criteria to achieve minimum $R_{on,sp}$.

IV. CONCLSUION

A 2D analytical modeling of breakdown voltage and on-resistance of GaN lateral LPSJ has been presented. The breakdown voltage of GaN LPSJ is obtained by solving impact ionization integral along the critical electric filed path with the modeling of the electric filed. Design examples with BV and minimum $R_{on,sp}$ at different x_{Al} composition have been discussed, providing valuable guidelines for the development of LPSJ.

ACKNOWLEDGMENT

This work is in part supported by the ARPA-E SWITCHES project.

REFERENCES

[1] H. Nie, S. Member, Q. Diduck, B. Alvarez, A. P. Edwards, B. M. Kayes, S. Member, M. Zhang, G. Ye, T. Prunty, D. Bour, and I. C. Kizilyalli, "1.5 KV and 2.2 mohm.cm^2 GaN transistors on Bulk-GaN Substrates," *IEEE Electron Device Lett.,*vol. 35, no. 9, pp. 939–941, 2014.

[2] Z. Tang, Q. Jiang, Y. Lu, S. Huang, S. Yang, X. Tang, and K. J. Chen, "600-V normally off SiNx/AlGaN/GaN MIS-HEMT with large gate swing and low current collapse," *IEEE Electron Device Lett.*, vol. 34, no. 11, pp. 1373–1375, 2013.

[3] M. Ishida, T. Ueda, T. Tanaka, and D. Ueda, "GaN on Si Technologies for Power Switching Devices," *IEEE Trans. Electron Devices*, vol. 60, no. 10, pp. 3053–3059, 2013.

[4] M. Zhu, B. Song, M. Qi, Z. Hu, K. Nomoto, X. Yan, Y. Cao, W. Johnson, E.Kohn, D. Jena and H. G. Xing, "1.9 kV AlGaN/GaN Lateral Schottky Barrier Diodes on Silicon," *IEEE Electron Device Lett.*, 2015 in press.

[5] T. Fujihira, "Theory of semiconductor superjunction devices," *Japanese Journal of Applied Physics*, vol. 36. pp. 6254–6262, 1997.

[6] T. Nitta, T. Minato, M. Yano, a. Uenisi, M. Harada, and S. Hine, "Experimental results and simulation analysis of 250 V super trench power MOSFET (STM)," *Proc ISPSD,* May 2000, pp. 77–80.

[7] L. Lorenz, G. Deboy, a. Knapp, and M. Marz, "COOLMOS^{TM}-a new milestone in high voltage power MOS," *Proc ISPSD,* May 1999, pp.3-10.

[8] Z. Li and T. P. Chow, "Design and Simulation of 5 – 20-kV GaN Enhancement-Mode Vertical Superjunctions HEMT," *IEEE Trans. Electron Devices*, vol. 60, no. 10, pp. 3230–3237, 2013.

[9] H. Ishida, D. Shibata, H. Matsuo, M. Yanagihara, Y. Uemoto, T. Ueda, T. Tanaka, and D. Ueda, "GaN-based natural super junction diodes with multi-channel structures," in *Proc. IEDM*, Dec 2008.

[10] B. Song, M. Zhu, Z. Hu, E. Kohn, D. Jena, and H. G. Xing, "GaN lateral PolarSJs□: polarization-doped super junctions," *Proc. 72th Annu. DRC, Jun. 2014*, pp. 3–4.

[11] D. Jena, S. Heikman, D. Green, D. Buttari, R. Coffie, H. Xing, S. Keller, S. DenBaars, J. S. Speck, U. K. Mishra, and I. Smorchkova, "Realization of wide electron slabs by polarization bulk doping in graded III-V nitride semiconductor alloys," *Appl. Phys. Lett.*, vol. 81, pp. 4395–4397, 2002.

[12] J. Simon, V. Protasenko, C. Lian, H. Xing, and D. Jena, "Polarization-induced hole doping in wide-band-gap uniaxial semiconductor heterostructures.," *Science*, vol. 327, no. 2010, pp. 60–64, 2010.

[13] J. Guo, G. Li, F. Faria, Y. Cao, R. Wang, J. Verma, X. Gao, S. Guo, E. Beam, A. Ketterson, M. Schuette, P. Saunier, M. Wistey, D. Jena, and H. Xing, "MBE-regrown ohmics in InAlN HEMTs with a regrowth interface resistance of 0.05□Ω.mm," *IEEE Electron Device Lett.*, vol. 33, no. 4, pp. 525–527, 2012.

[14] G. Li, R. Wang, B. Song, J. Verma, Y. Cao, S. Ganguly, A. Verma, J. Guo, H. G. Xing, and D. Jena, "Polarization-induced GaN-on-insulator E/D Mode p-channel heterostructure FETs," *IEEE Electron Device Lett.*, vol. 34, no. 7, pp. 852–854, 2013.

[15] G. M. Strollo and E. Napoli, "Optimal ON-resistance versus breakdown voltage tradeoff in superjunction power devices: A novel analytical model," *IEEE Trans. Electron Devices*, vol. 48, no. 9, pp. 2161–2167, 2001.

[16] E. Napoli, H. W. H. Wang, and F. Udrea, "Analytical calculation of the breakdown voltage for balanced, symmetrical superjunction power devices," *Proc ISPSD, Jun 2010*, pp. 205–208.

[17] L. Yu and K. Sheng, "Modeling and Optimal Device Design for 4H-SiC Super-Junction Devices," *IEEE Trans. Electron Devices*, vol. 55, no. 8, pp. 1961–1969, 2008.

[18] B. J. Baliga, "Gallium nitride devices for power electronic applications," *Semicond. Sci. Technol.*, vol. 28, p. 074011, 2013.